Photonic-crystal mediated charged particle beam velocity modulation and electromagnetic wave generation

2012 New J. Phys. 14 013014

(http://iopscience.iop.org/1367-2630/14/1/013014)

New Journal of Physics
The open-access journal for physics

Photonic-crystal mediated charged particle beam velocity modulation and electromagnetic wave generation

Yiming Xu[1,3] **and Rebecca Seviour**[2]

[1] Physics Department, Lancaster University, Lancaster LA1 4YB, UK
[2] University of Huddersfield, Queensgate, Huddersfield HD1 3DH, UK

New Journal of Physics **14** (2012) 013014 (7pp)
Received 7 November 2011
Published 11 January 2012
Online at http://www.njp.org/
doi:10.1088/1367-2630/14/1/013014

Abstract. We present the first experimental results of a photonic crystal (PC) structure-mediated charged particle beam velocity modulation and energy exchange. Our structure was based on two photonic lattices working at 9.532 GHz: a modulation lattice (ML) driven by a 2.5–6 W signal to velocity-modulate an electron beam of dc voltage from 15 to 30 kV and current from 50 to 150 μA, and an excitation lattice (EL) to exchange energy with the modulated beam, similar to a two-cavity klystron. Experimental results successfully demonstrated high spectral purity from signals excited by the velocity-modulated beam in the EL, with power level in excellent agreement with conventional theories.

A photonic crystal (PC) is a periodic arrangement of media with different refractive indices to form a lattice. Electromagnetic (EM) waves at certain frequencies can propagate through this lattice, but at other frequencies they cannot. The frequency regions where the wave can propagate are referred to as propagation bands, while the frequency regions where the wave cannot propagate are defined as band gaps [1]. Since the concept of PC was first introduced in 1987 [2, 3], PCs have been extensively studied, and demonstrated a range of novel physical phenomena [1], leading to a range of applications [1, 4], particularly in lasing, where defects in the lattice are used to produce intensely coherent radiation [4]. Recently, this technique was exploited by the authors of [5, 6], utilizing the high spectral purity of photonic structures to experimentally accelerate a charged particle beam, achieving an accelerating gradient of

[3] Author to whom any correspondence should be addressed.

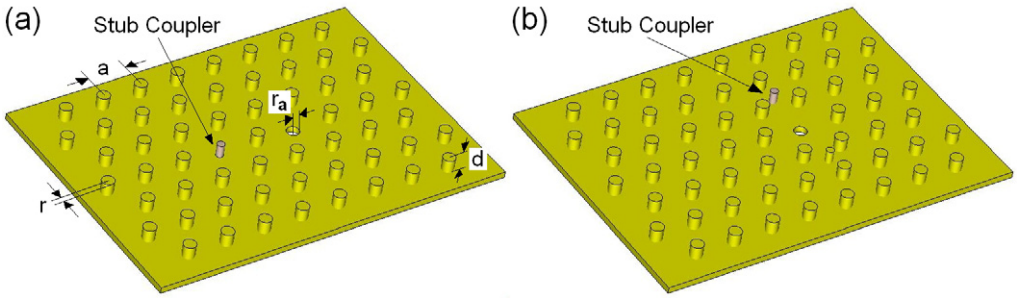

Figure 1. The design of (a) ML and (b) EL.

Table 1. Lattice design parameters.

Parameters	ML	EL
Rod radius (r)	1.995 ± 0.005 mm	2.013 ± 0.01 mm
Lattice constant (a)	12.50 mm	12.52 mm
Lattice depth (d)	3.6 mm	3.3 mm
Beam hole radius (r_a)	2 mm	2 mm

35 MV m^{-1}. The wakefields, as the EM fields induced in the PCs by traversing charged particles, were found in experiments to have minimized effects [7, 8].

Another potential use of PCs is in vacuum electronics; for example, the authors of [9] used an overmoded PC as a gyrotron resonator. The exceptional resonant state selectivity of PCs make them essential to overcome critical issues such as unwanted wakefield oscillations [10] in microwave power sources such as klystrons, in which EM fields are excited by a stream of continuous velocity-modulated electron bunches [11, 12]. Therefore, whether EM fields can be excited following conventional theories while maintaining high spectral purity in PCs by velocity-modulated beams is the first topic that has to be experimentally investigated. In this paper, we present our study on using a PC to velocity-modulate a charged particle beam to produce a continuous stream of electron bunches. We then demonstrate how these bunches can be used to excite a very pure EM signal in a second PC. The system we considered consists of two metallic PCs, each with a single defect, working as the modulation lattice (ML) and the excitation lattice (EL), respectively, at the same frequency, in a similar manner to a two-cavity klystron. The ML was fed by an external signal to excite a monopole (TM_{010}-like) resonant state at the defect. Electrons in a dc electron beam traversing the ML defect seeing different phases of the resonant electric fields are accelerated or decelerated, forming a continuously periodic velocity variation along the beam, which causes a bunching effect after a certain distance. The velocity-modulated beam excited EM fields at the same frequency in the EL defect, producing a continuous stable output signal.

The ML and EL are shown in figures 1(a) and (b), respectively, following the parameters presented in table 1. The lattices are based on a 2D triangular periodic array of metallic scatterers (rods) in air, with rod radius–spacing ratio 0.1596 and 0.1608, respectively, which was proved by the authors of [5] to confine only a TM_{010}-like state in each defect. To couple EM waves into and out of each lattice, stub couplers were used, formed by a scatterer of 1.27 mm diameter electrically isolated from each lattice, with a depth of $d/2$. In the ML, the coupler was placed

Table 2. Lattice characterization parameters.

Parameters	ML	EL
Central frequency (HFSS)	9.529 GHz	9.527 GHz
Measured resonant frequency	9.532 GHz	9.532 GHz
Reflection (S_{11})	0.004	0.135
Bandwidth	11.6 MHz	12.2 MHz
Propagation band	12.95 GHz	12.94 GHz
Loaded Q-factor (Q_L)	820	780
Ohmic Q-factor (Q_0)	1640	1790
External Q-factor (Q_e)	1640	1380
Shunt impedance (R_{sh})	74710 Ω	81190 Ω
R_{sh}/Q_0	45.55 Ω	45.36 Ω

two lattice constants away from the defect. In the EL, the coupler was placed besides the defect, 1.155 lattice constants away from the defect centre, as a small perturbation. The stub-coupled approach maintains the integrity of the lattices, preserving the high spectral purity of the lattice.

Each lattice was machined from high-conductivity oxygen-free copper using the parameters in table 1, with maximal fabrication errors of 10 μm in the lattice separation, which corresponds to a maximum shift in the resonant frequency of the defect of several MHz [13].

The ML and EL were characterized using an Agilent E8362B network analyser, by measuring the resonant frequencies, S-parameters (S_{11}), half-power bandwidths and frequency ranges of the propagation bands. The shunt impedances (R_{sh}, R_{sh}/Q_0) across the lattice gaps, as well as the ohmic, external and loaded quality factors, relating to power losses in the lattices, external loads and the whole loaded lattices, were also calculated. The parameters are presented in table 2, showing that at 9.532 GHz, the ML is critically coupled ($S_{11} = 0.004$) and the EL is slightly over coupled ($S_{11} = 0.135$). The S_{11} curve of the EL is plotted in figure 2. Comparison with Eigenmode results from the Ansys finite element method (FEM) based software, HFSS, and band diagrams computed from BandSOLVE[4] shows very good agreement.

EM field confinement and wave propagation in each lattice were characterized by measuring the power radiated from the lattice using small probes completely outside the lattice. At each frequency, the probes were swept around the outside edge of the lattice. Figure 2(c) shows that for frequencies in the propagation band the EM wave propagates through the lattice. For frequencies in the band gap, an EM response was observed only in the defect region, as indicated by the S_{11} curve. This response was found to be highly localized to the defect; outside of the defect the field was negligible.

The axial electric field along the axis of the defect in each PC (E_z) was measured using a bead-pull perturbation technique [14]. Figure 3 shows the experimentally measured E_z and the numerical results, both normalized to 1 W using the measured ohmic Q-factor (Q_0) from table 2. As seen in figure 3, the experimental results are in good agreement with the numerical results, where the maximum variation is 3.5%. The R_{sh}/Q_0 in table 2 for each PC was calculated

[4] BandSOLVE Manual 2008 (RSoft Design Group).

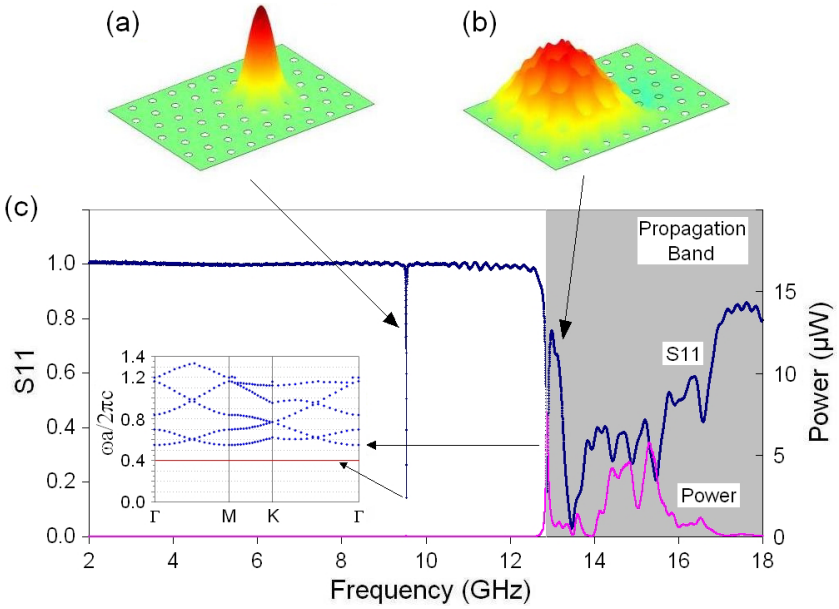

Figure 2. The EL: (a) monopole state confined at defect region (HFSS = 9.527 GHz, measurement = 9.532 GHz); (b) first higher-order state at propagation band (HFSS = 13.03 GHz); (c) measured S_{11} and power leakage compared with band diagram.

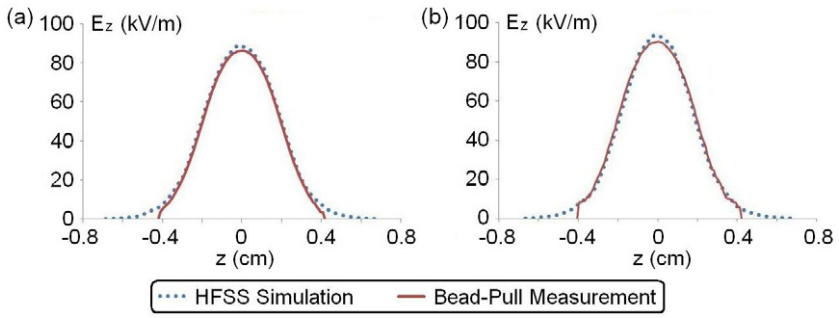

Figure 3. Bead-pull measurements of axial field strengths compared with HFSS simulation results in the (a) ML and (b) EL.

from the corresponding E_z following the definition in [11, 12]:

$$\frac{R_{\mathrm{sh}}}{Q_0} = \frac{|V_{\mathrm{g}}|^2}{2\omega U_0} = \frac{\left(\int_{-\infty}^{\infty} |E_z| \mathrm{d}z\right)^2}{2\omega U_0}, \tag{1}$$

where $V_{\mathrm{g}} = \int_{-\infty}^{\infty} E_z \, \mathrm{d}z$ is the PC axial gap voltage and U_0 is the total energy stored in the PC.

The two lattices are separated by 125 mm, embedded in a series of focusing coils, as shown in figure 5(a). This separation forms a drift space for the beam to velocity-modulate, as illustrated in figure 4(a). Figure 4 was produced using the particle-in-cell (PIC) code VORPAL, simulating the velocity modulation effect of a 20 kV, 100 μA electron beam with an initial spot size of 3 mm, interacting with a 9.532 GHz, 2.5 W EM field excited in the defect region of the ML, under a small magnetic focusing field of 5 mT. Figure 4 also shows the evolution of

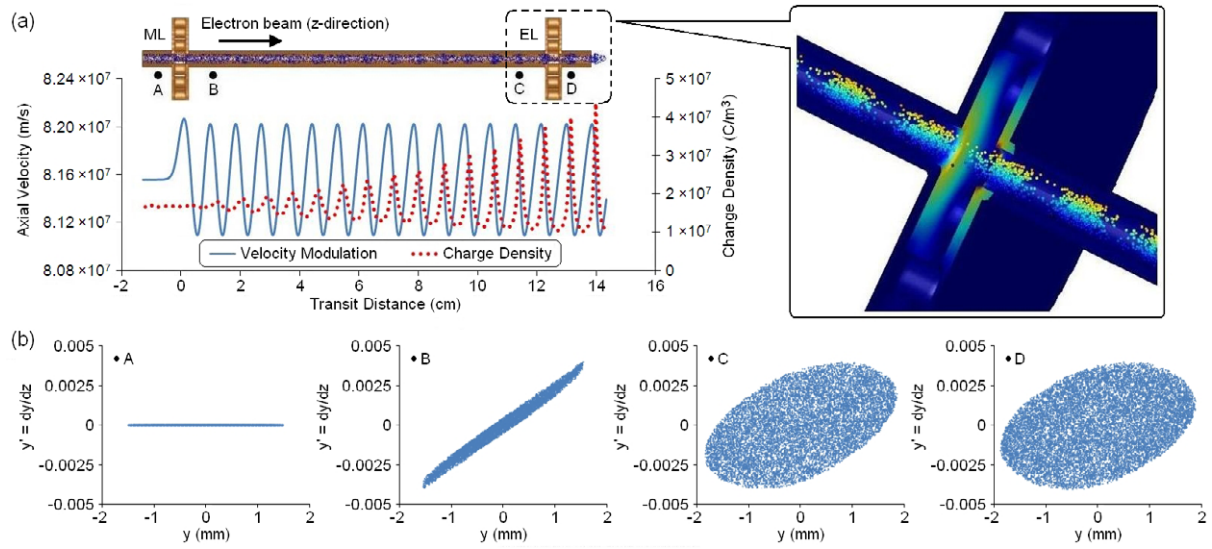

Figure 4. Velocity-modulated beam dynamics: (a) beam profile, velocity modulation and charge density distribution; (b) beam transverse phase-space plots at points A, B, C and D.

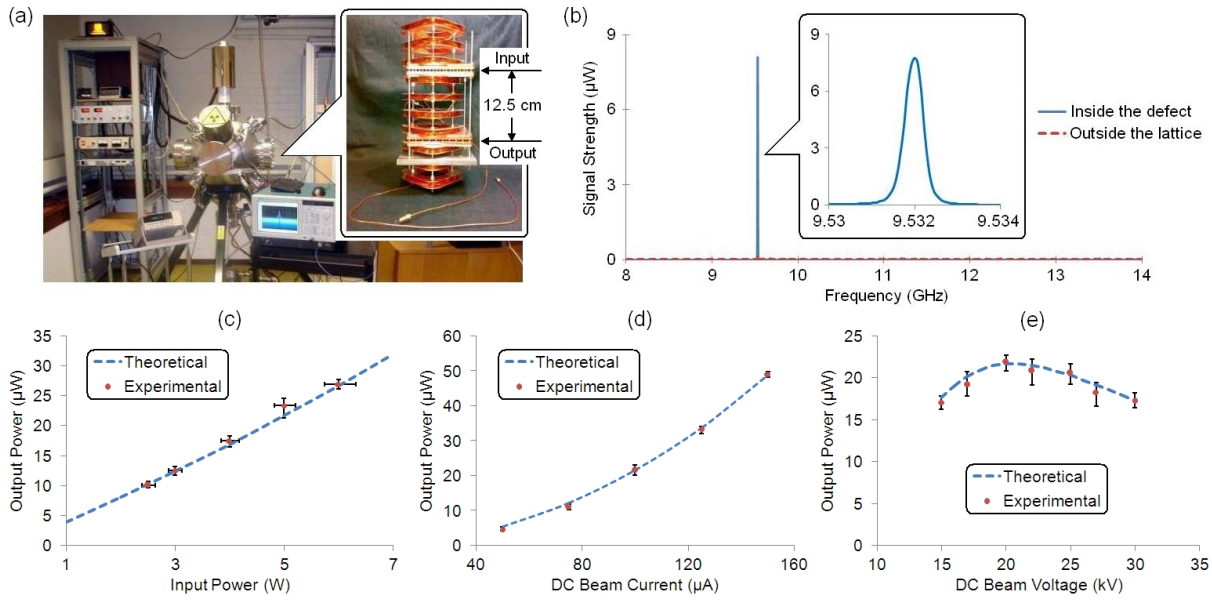

Figure 5. Proof-of-principle experimental setup and results. (a) The two-PC module and experimental system setup. (b) Spectrum of output signal excited by a beam of $V_{dc} = 20\,\text{kV}$ and $I_{dc} = 100\,\mu\text{A}$, modulated by an EM field in ML of $P_{in} = 2.5\,\text{W}$ at 9.532 GHz. (c) P_{out} versus P_{in} at 9.532 GHz, at $V_{dc} = 20\,\text{kV}$ and $I_{dc} = 100\,\mu\text{A}$. (d) P_{out} versus I_{dc} at $V_{dc} = 20\,\text{kV}$ and $P_{in} = 5\,\text{W}$ at 9.532 GHz. (e) P_{out} versus V_{dc} at $I_{dc} = 100\,\mu\text{A}$ and $P_{in} = 5\,\text{W}$ at 9.532 GHz.

the beam profile, axial velocity modulation and charge density distribution at saturation. The strength of the EM field excited by the modulated beam in the EL defect was significantly limited by the low beam current. Hence the energy exchanged from the electron bunches to the

EM field was small [11]. This is seen from the almost constant velocity modulation (figure 4(a)). The low beam current also means that the effect of space charge is negligible [11, 12], giving rise to a stable increment in the peak charge density as seen in figure 4(a).

The radial components of the EM field at the ML cause an increment in the radial velocity of the beam, causing the beam to spread (i.e. emittance growth). Figure 4(b) shows the beam transverse phase-space plots at the centre of the bunch at different points along the structure in figure 4(a). We see that the transverse beam velocities immediately increased after interaction with the bunching signal (B). During the drift distance between points B and C the space-charge forces are maximum at the peak charge density, causing the beam to spread (C). The beam transverse movement maintains a natural increment after interacting with the weak EM fields in the EL defect (D). The peak beam radius (r_b) increased by approximately 25% along the whole drift length.

The experimental system setup is shown in figure 5(a). The photonic module was mounted in a vacuum chamber, with an electron gun emitting a beam (10–30 kV, 0–1 mA) through the photonic module. The EM field in the ML was created by a TMD PTX8206 power module, delivering a 2.5–6 W EM field at 9.532 GHz. The EL was connected to an Anritsu ML2487A power meter and a Tektronix RSA6114A real-time spectrum analyser, to analyse the output power and spectrum, respectively. When the electron beam was switched off, there was no EM field observed in the EL. When the electron beam was switched on, an EM field excited by the modulated beam in the EL was observed to peak at the same frequency as the input signal (9.532 GHz), as shown in figure 5(b). The spectrum of this EM field has a very narrow bandwidth of 497 kHz and a very small uncertainty of less than 1%, indicating very good signal purity.

As the higher-order harmonics are not confined in the lattices, they are not expected to be efficiently excited. The authors of [8] successfully demonstrated in experiment that the Q-factors of higher-order harmonics in PCs are much lower than the confined TM_{010}-like state via a single bunch sweep. In our experiment, the electron beam was velocity-modulated to the frequency of the TM_{010}-like state (9.532 GHz); this indicated that the higher-order harmonics (at 13.03 GHz and above) largely lose synchronization with the beam. According to Uhm's theorem [15] this further suppresses the higher-order harmonics. This is proved by our output spectrum measurement from 8 to 14 GHz as shown in figure 5(b); no higher-order spectrum is observed either from the output stub coupler next to the defect inside the EL or from a probe outside the entire EL. The spectrum of the higher-order harmonics is below the noise level measurable by the spectrum analyser, which is 26 dB lower than the peak at 9.532 GHz.

The beam velocity modulation effect was examined by measuring the dependence of output power (P_{out}) versus input power at the ML (P_{in}), dc beam current (I_{dc}) and voltage (V_{dc}). The results are shown in figure 5, in comparison with theoretical calculation based on the two-cavity klystron theory [11, 12]:

$$P_{out} = \frac{1}{2}(M_2|i|)^2 Q_L \left(\frac{R_{sh}}{Q_0}\right)\left(\frac{Q_L}{Q_e}\right) \tag{2}$$

where the magnitude of the radio frequency (RF) component of the modulated beam current ($|i|$) is [11]

$$|i| = \frac{1}{2} M_1 \frac{I_{dc}}{V_{dc}} \frac{\omega}{\omega_q} |\sin(\beta_q z)||V_1|, \tag{3}$$

with $|V_1|$ being the magnitude of the voltage across the gap of the ML and ω_q and β_q are the reduced plasma frequency and wavenumber, respectively, [11, 12]. In this analysis, we

have considered the effect of beam-loading to be negligible due to the low beam current used [11, 12].

In equations (2) and (3), the subscripts 1 and 2 stand for relevant parameters of the ML and EL, respectively, referring to tables 1 and 2. M is the beam coupling coefficient, which describes how well energy is extracted from or given to the electron beam by the lattices [11, 12]:

$$M_i = J_0\left(\frac{\omega d_i}{2v_0}\right)\frac{\sqrt{I_0^2(\gamma r_\mathrm{b}) - I_1^2(\gamma r_\mathrm{b})}}{I_0(\gamma r_a)}, \tag{4}$$

in which v_0 is the initial beam velocity and γ is the free-space radial propagation factor [11]. $J_0(x)$, $I_0(x)$ and $I_1(x)$ are original and modified Bessel functions. The subscript $i = 1, 2$ represents M for ML and EL.

As seen in figure 5, the experimental results are in agreement with theoretical calculations. For very low I_dc and limited drift distance, the photonic module presents a linear response to P_in from 2.5 to 6 W, shown in figure 5(c). In figure 5(d), the slightly increased trend of P_out indicates that the beam undergoes a spatial spreading with increasing I_dc due to space-charge effects. In figure 5(e), the maximum P_out was measured at $V_\mathrm{dc} = 20$ kV, as predicted. The larger error range is primarily due to the variation in beam diameter with V_dc.

In conclusion, we have successfully demonstrated experimentally that a photonic lattice can velocity-modulate a charged particle beam and that this modulated beam can continuously excite EM waves in another lattice. The generated EM wave benefited from the high spectral purity that PCs naturally possess. The dependence of the spectrum excited in the EL on the beam properties has been shown to agree with conventional theory, verifying the possible use of photonic structures in conventional vacuum electronics.

References

[1] Joannopoulos J D, Johnson S G, Winn J N and Meade R D 2008 *Photonic Crystals: Molding the Flow of Light* 2nd edn (Princeton and Oxford: Princeton University Press)

[2] Yablonovitch E 1987 *Phys. Rev. Lett.* **58** 2059

[3] John S 1987 *Phys. Rev. Lett.* **58** 2486

[4] Busch K, Lolkes S, Wehrspohn R B and Foll H 2004 *Photonic Crystals: Advances in Design, Fabrication and Characterization* (Weinheim: Wiley-VCH)

[5] Smirnova E I, Mastovsky I, Shapiro M A and Temkin R J 2005 *Phys. Rev. ST – Accel. Beams* **8** 091302

[6] Smirnova E I, Kesar A S, Mastovsky I, Shapiro M A and Temkin R J 2005 *Phys. Rev. Lett.* **95** 074801

[7] Marsh R A, Shapiro M A, Temkin R J and Smirnova E I 2007 *Proc. PAC07* p 3002

[8] Jing C *et al* 2009 *Phys. Rev. ST – Accel. Beams* **12** 121302

[9] Sirigiri J R, Kreischer K E, Machuzak J, Mastovsky I, Shapiro M A and Temkin R J 2001 *Phys. Rev. Lett.* **86** 5628

[10] Krietenstein B, Ko K, Lee T, Becker U, Weiland T and Dohlus M 1995 *Proc. 1995 IEEE Particle Accelerator Conf.* p 1533

[11] Caryotakis G 2005 *High Power Klystrons: Theory and Practice at The Stanford Linear Accelerator Center, Part I* (Stanford Linear Accelerator Center, Menlo Park, CA 94025, San Mateo, CA, USA)

[12] Smith M J and Phillips G 1995 *Power Klystrons Today* (Taunton: Research Studies Press)

[13] Matthews C J and Seviour R 2008 *Appl. Phys.* B **94** 381

[14] Xu Y and Seviour R 2010 *Proc. IPAC'10* p 4002

[15] Uhm H S, Park G S and Armstrong C M 1993 *Phys. Fluids* B **5** 1349